I&EC research
Industrial & Engineering Chemistry Research

Article

pubs.acs.org/IECR

Investigation of Variable Impurity Profile from a Mitsunobu Reaction Using Insights from Kinetic Modeling, Multi-Phase Interactions, and Computational Fluid Dynamics

Samrat Mukherjee,* Shailendra Bordawekar, and Nandkishor Nere

Process Research and Development, AbbVie Inc., 1 North Waukegan Road, North Chicago, Illinois 60064, United States

ABSTRACT: A drug substance intermediate synthesis involving a Mitsunobu coupling reaction using triphenylphosphine and diisopropyl azodicarboxylate was investigated to understand the variable levels of an impurity. One of the precursors for the impurity, 1,2-isopropylhydrazine dicarboxylate (a reaction byproduct), crystallizes out of the reaction medium and also forms a cocrystal with triphenylphosphine oxide (TPPO), another reaction byproduct. The dynamic byproduct concentrations as a result of these phenomena were taken into account in a reaction kinetics model. The variability in impurity formation was linked to the concentration of 1,2-isopropylhydrazine dicarboxylate, which is dependent on reaction progress and 1,2-isopropylhydrazine dicarboxylate−TPPO cocrystal formation. The cocrystal formation is in turn affected by the mixing characteristics in the reactor. Computational fluid dynamics simulation of the mixing patterns and a series of proof-of-concept experiments were performed to establish the influence of mixing intensity and cocrystal formation on the level of impurity formed.

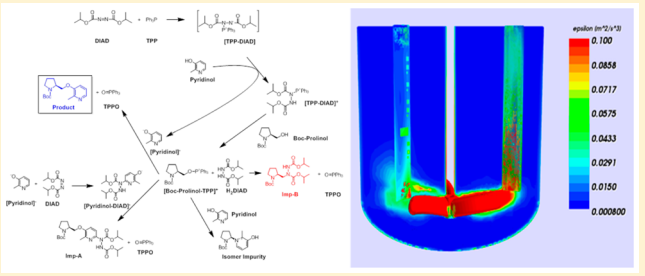

1. INTRODUCTION

In the pharmaceutical industry, control of impurities in the manufacture of drug substance is a critical aspect that requires significant R&D efforts from chemists and chemical engineers. The control strategy for impurities can be formulated on the basis of control at the source of formation, control via downstream removal, control through raw materials, or a combination of these. As the R&D team progresses through the drug development timeline, there is need to manufacture larger quantities of drug substance in order to supply drug for the clinical studies even before a final control strategy is established. The scale of manufacture at this stage may range from a few kilograms to a few hundreds of kilograms depending on the type of drug and indication; and this requires scaleup from laboratory to a pilot plant or a larger manufacturing facility.

Typically, chemical reactions that are homogeneous, once studied in adequate detail through laboratory development work present minimal scale up issues. However, mass transfer considerations become important during scale up for heterogeneous reactions, where one or more of the reactants or a catalyst is in a different phase than the reaction medium. If product insolubility is the reason for heterogeneity then depending on crystallization or precipitation characteristics of the product and likelihood of entraining impurities in that process, the level of scrutiny needed during scale up may vary. The case study presented here is different from either of the above scenarios since the reactants and products (including impurities) are in the same liquid phase, while reaction byproducts crystallize out. While the crystallization of the reaction byproducts offers a significant benefit in terms of purification, one of the reaction byproducts is linked to the formation of a process impurity. The variability in the crystallization behavior of this byproduct results in variations in its solution concentration, thereby affecting the product purity.

Determination of reaction kinetics has become a mainstream activity in pharmaceutical process development due to the greater depth of understanding that can be achieved in terms of cause and effect relationships between reaction parameters such as temperature, concentration, stoichiometry, and product characteristics such as yield and purity. Reaction kinetics analysis also elucidates multivariate interactions among reaction parameters. This knowledge often affords optimization of reaction parameters toward a given objective or a set of objectives involving product throughput, impurity limits, cycle time, reagent quantities, waste generation, and safety considerations. The level of understanding sought from a reaction kinetics model is often dictated by the ability to detect and measure species, including reaction intermediates. In a fit-for-purpose industrial research environment, better analytics are developed and more data is available to use in building more sophisticated models as a program matures. For instance, projects in early stages of process development may rely on simpler approaches, whereas those in late-stage commercial

Received: January 26, 2016
Revised: April 4, 2016
Accepted: April 11, 2016

DOI: 10.1021/acs.iecr.6b00344
Ind. Eng. Chem. Res. XXXX, XXX, XXX−XXX

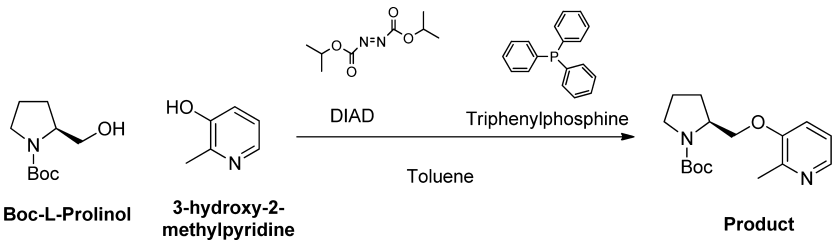

Figure 1. Mitsunobu coupling reaction.

development may resort to detailed understanding of physicochemical phenomena.

The current case study involves an early stage project where the key reaction in the production of a drug substance intermediate was exhibiting significant variability in impurity formation with changes in scale and equipment. The reaction under consideration is a Mitsunobu-type coupling using triphenylphosphine (TPP) and diisopropyl azodicarboxylate (DIAD) as the redox agents, as shown in Figure 1.

The Mitsunobu reaction is widely used in organic synthesis for conversion of primary and secondary alcohols to esters, ethers, and other compounds.[1,2] This is achieved by substituting the alcohol with nucleophiles, mediated by a redox combination of a trialkyl- or triarylphosphine and a dialkyl azodicarboxylate. In the present case, Boc-*L*-prolinol (the alcohol species) is coupled with 3-hydroxy-2-methylpyridine (pyridinol, hereinafter), using triphenylphosphine (TPP) and diisopropyl azodicarboxylate (DIAD) as the redox agents.

The chemical structures of key impurities and byproducts generated in the above reaction are presented in Figure 2. The

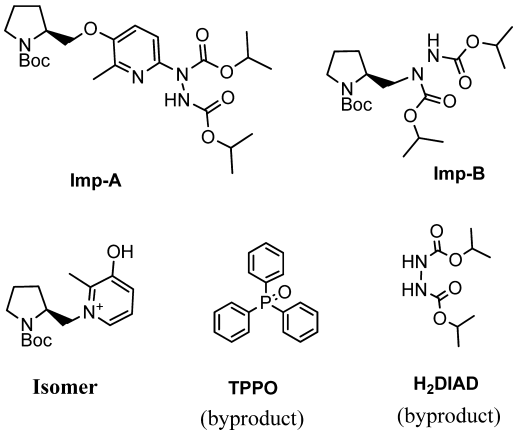

Figure 2. Structures of key coupling impurities and reaction byproducts.

isomer impurity is a result of *N*-alkylation of the pyridinol as opposed to *O*-alkylation that yields the desired product. Imp-A, the DIAD-adduct of the product, is formed when DIAD-adduct of pyridinol, instead of normal pyridinol, goes through the coupling reaction. Imp-B is the DIAD adduct of Boc-*L*-prolinol. Triphenylphosphine oxide (TPPO) and reduced DIAD (H_2DIAD) are the reaction byproducts. Imp-B is particularly high, even under the most optimal reaction conditions. The initial set of data generated in the laboratory under nominal conditions indicated consistent formation of Imp-B in the 2–3% range, which was acceptable in terms of the ability to purge downstream to an acceptable level in the final drug substance. However, upon moving to larger scale, we observed considerable variability in the level of Imp-B using the same procedure. This study focuses primarily on understanding the formation of the product and Imp-B.

2. RESULTS AND DISCUSSION

2.1. Proposed Reaction Mechanism. Although the Mitsunobu reaction is commonly used, the mechanistic details are widely debated, especially around the active intermediates.[3−7] In this study, a broadly accepted mechanism was used to build a reaction kinetics model.

Figure 3 shows the network of reaction pathways leading to product and impurities formation. The first step in the reaction pathway involves the extremely rapid reaction of TPP and DIAD to form a betaine species, [TPP-DIAD] zwitterion, which has been well-established in the literature.[5] This zwitterion abstracts a proton from pyridinol, and the resulting $[TPP\text{-}DIAD]^+$ species attacks the Boc-*L*-prolinol species to form an activated species and H_2DIAD. The activated Boc-prolinol can generate the product and the impurities to the extent governed by chemical kinetics.

Another important aspect to consider in the discussion of reaction mechanism is the reaction protocol, especially for this type of reaction where a different pathway may operate when the order of addition of the reagents is changed.[8] It is recommended to have both the alcohol and the nucleophile (here, Boc-*L*-prolinol is the alcohol and pyridinol is the nucleophile) in the system prior to formation of [TPP-DIAD] complex to minimize undesirable reactions. Therefore, a protocol was developed as follows. Boc-*L*-prolinol (limiting reactant), pyridinol (1.15 mol equiv), TPP (1.21 mol equiv), and toluene (6.0 kg/kg Boc-*L*-prolinol) are first charged to a dry reactor. The jacket on the reactor is set to −15 °C. Upon reaching a steady subzero internal temperature, DIAD (95% purity, 1.1 mol equiv) is added via a dip-tube over 3 h such that the internal temperature is maintained at subzero. The reaction mixture is then warmed up to 25 °C over a 3 h period and aged for the reaction to proceed. The mixture of reagents in toluene prior to DIAD addition is heterogeneous, and by the end of the DIAD addition, the system is almost homogeneous with some undissolved pyridinol. Solubility measurements of pyridinol in the reaction medium indicate that as the temperature is raised to 25 °C, the medium has the capacity to dissolve most of the pyridinol.

The instantaneous formation of [TPP-DIAD] implies that if DIAD is used in stoichiometric excess to TPP (i.e., TPP:DIAD < 1) then available DIAD can react with $[pyridinol]^-$ to form $[pyridinol\text{-}DIAD]^-$ adduct, leading to Imp-A formation. Therefore, Imp-A is easily controlled by maintaining the ratio: TPP:DIAD > 1, as illustrated by the experimental observations in Table 1. As the TPP:DIAD ratio decreases, the level of Imp-A increases.

DOI: 10.1021/acs.iecr.6b00344
Ind. Eng. Chem. Res. XXXX, XXX, XXX−XXX

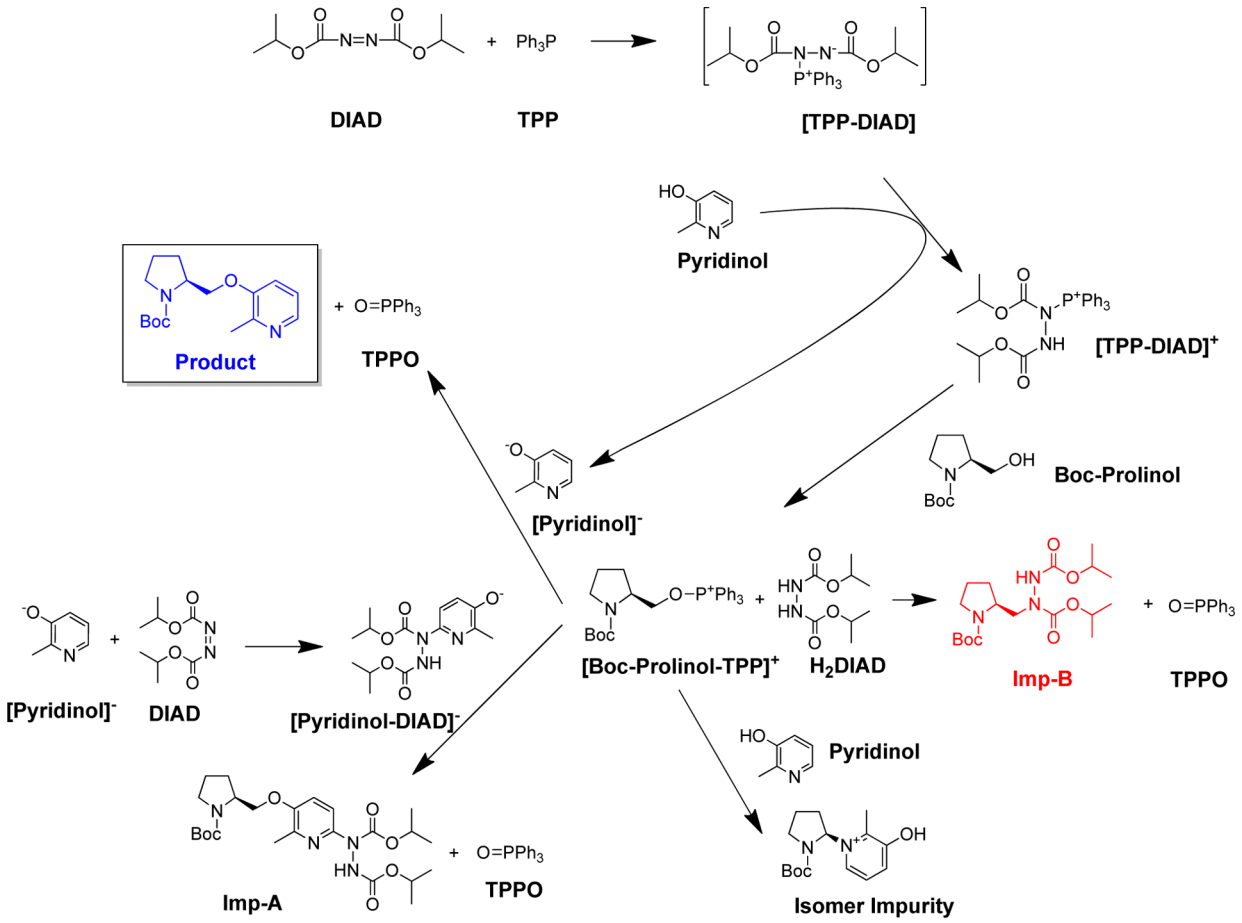

Figure 3. Proposed reaction pathways leading to formation of product and impurities.

Table 1. Influence of TPP:DIAD Molar Ratio on Imp-A Formation[a]

TPP (equiv)	DIAD (equiv)	TPP:DIAD	Imp-A (wt %)
1.21	1.10	1.10	0.10%
1.18	1.14	1.04	0.14%
1.14	1.14	1.00	2.01%
1.10	1.14	0.96	3.87%
1.0	1.50	0.67	74.60%

[a]All reagents are quoted relative to moles of Boc-L-prolinol starting material. Nominal quantity of pyridinol (1.15 mol equiv) was used in each case.

Table 2. Influence of Pyridinol Stoichiometry on Isomer Impurity Formation[a]

TPP (equiv)	pyridinol (equiv)	pyridinol:TPP ratio	isomer impurity (wt %)
1.2	1.2	1.0	1.9%
1.5	2.0	1.3	7.7%
1.5	3.0	2.0	16.2%

[a]The TPP:DIAD molar ratio in each case was greater than 1.

When excess pyridinol exists in the system relative to TPP and DIAD, neutral pyridinol can result in *N*-alkylation to form the isomer impurity. A set of experiments was performed where the TPP:DIAD molar ratio was greater than 1 to minimize Imp-A formation, and higher than nominal stoichiometric equivalents of pyridinol (nominal = 1.15 mol equiv) were used. As shown in Table 2, significant levels of isomer impurity are formed when pyridinol:TPP ratio is greater than one, and the level of isomer impurity increases with the increase in the pyridinol:TPP ratio.

Imp-B is formed when the activated Boc-*L*-prolinol, and H_2DIAD, both produced from the same reaction step, react further, as shown in Figure 3. The primary reason for this pathway is the high pK_a of pyridinol, thus creating a competition between [pyridinol]$^-$ and H_2DIAD for the activated Boc-prolinol species.[9] In fact, the formation of Imp-B exemplifies one of the drawbacks of Mitsunobu coupling of nucleophiles with low acidity (pK_a > 11). In this case, pyridinol plays the part of the nucleophile, and its pK_a is estimated to be 10.4 at the hydroxyl group (calculated value). As activated Boc-*L*-prolinol is the precursor to formation of both Imp-B and the product, manipulation of Boc-*L*-prolinol stoichiometry does not afford control on generation of Imp-B. Adding complexity to this system is the precipitation of the reaction byproducts, H_2DIAD and TPPO. The rate of formation and the total quantity of Imp-B formed will depend on the solution phase concentration of H_2DIAD. The primary focus of this investigation is to build an understanding of the reaction kinetics and factors impacting formation of Imp-B.

2.2. Kinetics Modeling. For the purpose of kinetics model development, the scope was restricted to the reaction steps leading to the product and Imp-B for two reasons: (a) the isomer impurity and Imp-A are well-controlled by straightforward control of reagent stoichiometry: pyridinol:TPP < 1 and TPP:DIAD > 1, respectively, and (b) the sum total of isomer

DOI: 10.1021/acs.iecr.6b00344
Ind. Eng. Chem. Res. XXXX, XXX, XXX−XXX

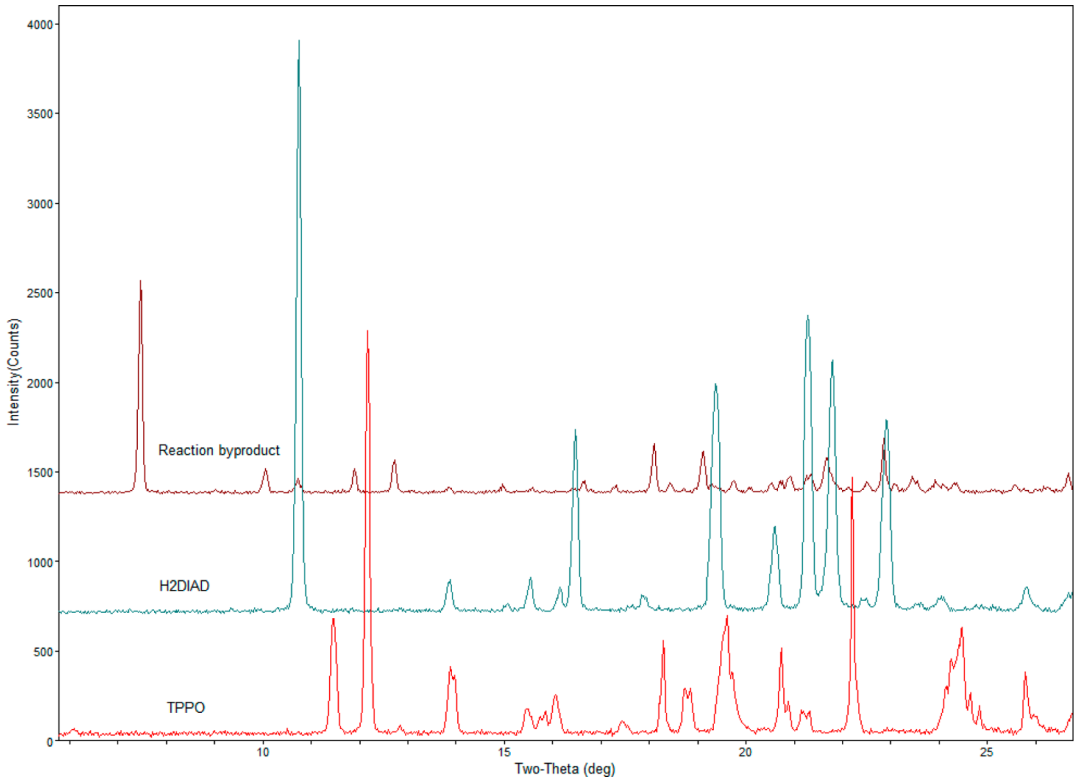

Figure 4. PXRD patterns for TPPO, H_2DIAD, and solid reaction byproduct confirming formation of the TPPO−H_2DIAD cocrystal.

impurity and Imp-A is < 1% when the above stoichiometric criteria are met. On the basis of the reaction network in Figure 3, the set of elementary reactions considered for model development is as follows:

Product Formation:

$$\text{TPP} + \text{DIAD} \xrightarrow{k_1} [\text{TPP} - \text{DIAD}] \quad (1)$$

$$[\text{TPP}-\text{DIAD}] + \text{pyridinol} \xrightarrow{k_2} [\text{pyridinol}]^- + [\text{TPP} - \text{DIAD}]^+ \quad (2)$$

$$[\text{TPP} - \text{DIAD}]^+ + \text{Boc-}L\text{ - prolinol} \xrightarrow{k_3} [\text{Boc-}L\text{-prolinol}-\text{TPP}]^+ + \text{H}_2 - \text{DIAD} \quad (3)$$

$$[\text{Boc-L-prolinol}-\text{TPP}]^+ + [\text{pyridinol}]^- \xrightarrow{k_4} \text{product} + \text{TPPO} \quad (4)$$

Imp-B Formation:

$$[\text{Boc-}L\text{-prolinol}-\text{TPP}]^+ + \text{H}_2\text{DIAD} \xrightarrow{k_5} \text{Imp} - \mathbf{B} + \text{TPPO} \quad (5)$$

Apart from the elementary reaction steps, it should be noted that both TPPO and H_2DIAD crystallize out of the reaction medium, which changes the solution phase concentration of H_2DIAD. TPPO is known to be an effective crystallization aid in organic chemistry literature through the formation of cocrystals.[10] In this case, the solid byproduct collected at the end of the reaction was found to be a cocrystal comprising of TPPO and H_2DIAD. The composition determined by HPLC indicated equimolar TPPO and H_2DIAD in the solid byproduct, and the presence of cocrystal was confirmed by powder X-ray diffraction (PXRD) analysis, which indicated a diffraction pattern different from either TPPO or H_2DIAD (see Figure 4). The equilibrium concentrations of TPPO and H_2DIAD were determined by measuring their respective liquid-phase concentrations in the reaction medium containing the TPPO−H_2DIAD cocrystal, as shown in Figure 5. However, when TPPO was added to a filtered aliquot of the reaction medium that was saturated with the cocrystal, a portion of the added TPPO dissolved in the medium. This result indicated a higher solubility for TPPO in the absence of the TPPO−H_2DIAD cocrystals compared to the equilibrium concentration of TPPO in the presence of the cocrystal. A similar result was also obtained in the case of H_2DIAD, as seen in Figure 5 from the higher values of liquid-phase concentrations in the absence of the cocrystal. Upon the formation of the cocrystal in the reaction medium, the liquid-phase concentrations of the constituents are governed by the lower equilibrium concentration values (solid symbols in Figure 5).

The solution phase equilibrium concentrations of TPPO and H_2DIAD in the presence and absence of cocrystal as functions of temperature were used to develop the kinetics model. A step change in the equilibrium concentration profile was incorporated for H_2DIAD when the Boc-*L*-prolinol conversion was 65%. This conversion value corresponds to a H_2DIAD concentration equivalent to the solubility of H_2DIAD in the presence of cocrystals at 25 °C. Since the equilibrium concentration data for TPPO and H_2DIAD were generated using the typical composition of reaction contents including the toluene solvent, the conversion threshold may vary from the

DOI: 10.1021/acs.iecr.6b00344
Ind. Eng. Chem. Res. XXXX, XXX, XXX−XXX

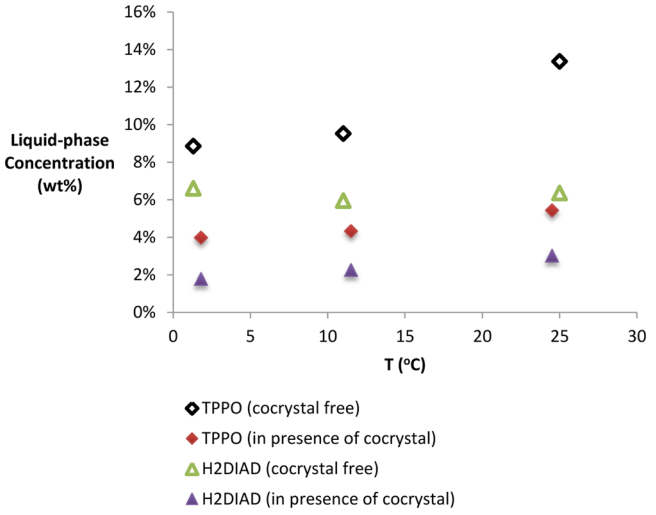

Figure 5. Equilibrium concentrations of TPPO and H_2DIAD as a function of temperature under two conditions: in the presence of cocrystal (filled symbols), and in the absence of cocrystal (empty symbols).

65% level if the reaction composition is altered. To minimize the level of complexity in the modeling effort, the mass-transfer coefficient, k_la, was set to a high value in the model, which implies instantaneous nucleation of the TPPO–H_2DIAD cocrystal without significant buildup of supersaturation.

The reaction steps (1–5) along with equilibrium concentration data for TPPO and H_2DIAD as a function of temperature were used to build a model using DynoChem. The data for regression of the rate parameters were derived from laboratory experiments. These reactions were conducted under a protocol where precooled DIAD is added to a subzero mixture of Boc-*L*-prolinol, pyridinol, TPP, and toluene. After the DIAD addition, the temperature is adjusted to 0 °C and then ramped up to 25 °C over 3 h. The reaction was sampled during the temperature ramp and through the subsequent multihour aging period and analyzed by HPLC for Boc-*L*-prolinol, product, Imp-A, and Imp-B. Imp-A levels were well under 1%, and as previously mentioned, the model was not developed to account for Imp-A.

The modeling results presented in Figure 6a indicate a reasonable fit of the data for the main reaction and formation of

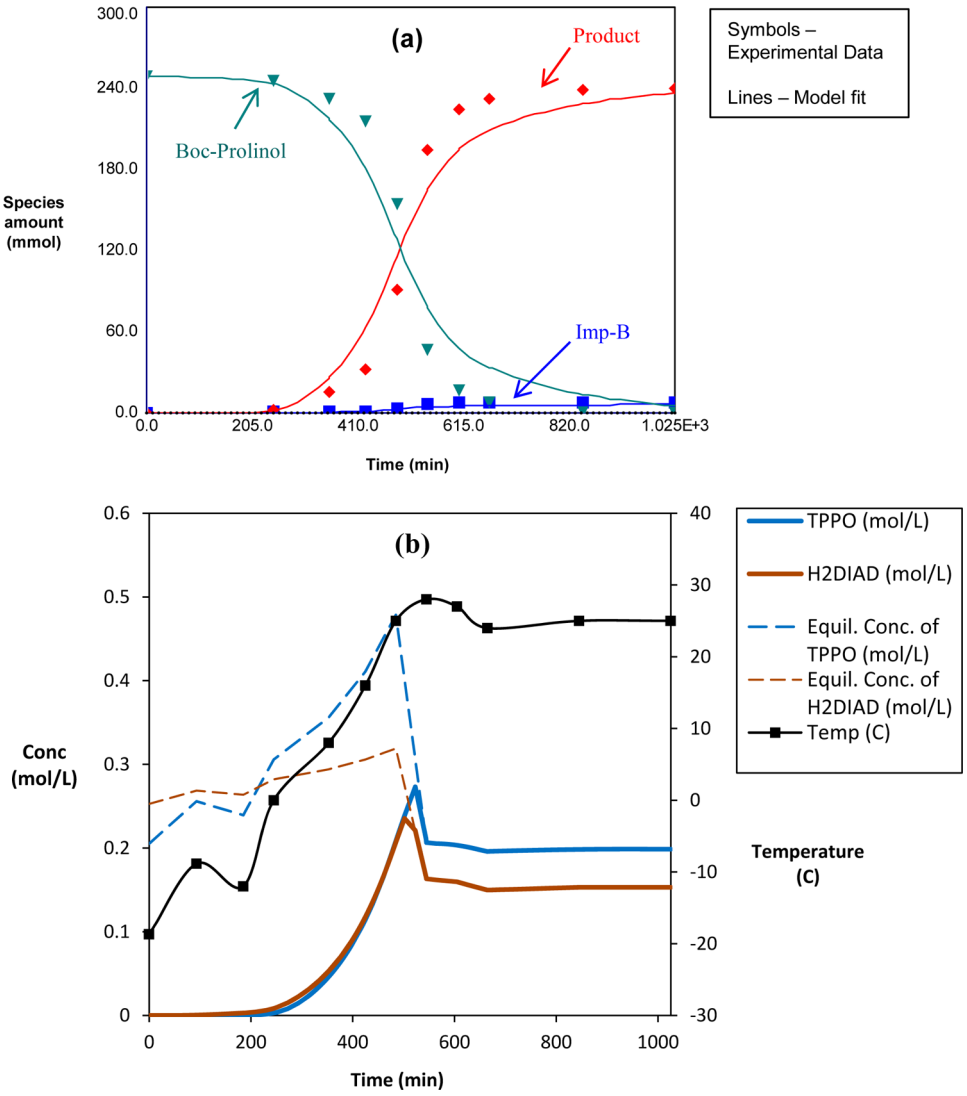

Figure 6. Modeling results: (a) Model fits (solid lines) for temporal concentration profiles of Boc-*L*-prolinol, product, and Imp-B. (b) Simulation of TPPO and H_2DIAD solution-phase concentrations (solid lines) during the reaction and comparison to equilibrium concentrations (dotted lines).

DOI: 10.1021/acs.iecr.6b00344
Ind. Eng. Chem. Res. XXXX, XXX, XXX–XXX

Imp-B. Figure 6b shows the imposed equilibrium concentration profiles for H_2DIAD and TPPO (dotted lines) as a function of temperature using the van't Hoff equation. The solid lines represent the simulated concentration profiles for H_2DIAD and TPPO as the reaction progresses. Between 485 and 545 min time points, when the conversion crosses the 65% mark, the profiles transition from the solubility in the absence of cocrystal to lower values as formation of the cocrystal results in a drop in the solution phase concentration of these species.[11]

The regressed rate parameters were the pre-exponential factor (A_0) and activation energy (E_{act}) for each of the rate constants per the expression, $k = A_0 \exp(-E_{act}/RT)$. In order to compare the rate constants of the five reactions, k-values calculated at the reference temperature of 25 °C are listed in Table 3.

Table 3. Regressed Rate Constants for reactions 1−5 from the Kinetics Model

rate constant at T_{ref} = 25 °C	regressed value (L/mol s)
k_1	1.00×10^{03}[a]
k_2	4.54×10^{-04}
k_3	4.74×10^{-03}
k_4	3.53×10^{-01}
k_5	1.93×10^{-03}

[a]A high value was fixed for k_1 (excluded from regression) to reflect the instantaneous reaction to form the betaine species. There is no sensitivity of the fixed k_1 value on k_2−k_5.

On the basis of the rate constants, the rate-determining step for the reaction sequence is the deprotonation of pyridinol (reaction 2). The pyridinol anion (in reaction 4) and H_2DIAD (in reaction 5) compete for the activated Boc-*L*-prolinol formed in reaction 3. The relative rate constant of reaction 4 with respect to reaction 5 (k_4:k_5) is 183, which is in line with the observation of a significant amount of product formed compared to Imp-B. Historical data on this reaction had established that lower reaction temperature results in extremely long reaction time and higher selectivity for Imp-B versus product. This is further supported by the activation energy values regressed from the model, 62 kJ/mol for reaction 4 versus 36 kJ/mol for reaction 5. Although higher reaction temperatures were favorable in terms of shorter reaction time and lower Imp-B level, addition of DIAD at a temperature higher than 0 °C was not a viable option due to formation of other impurities.

2.3. Effect of Reactor Scale and Geometry. As more effort was put in the overall drug substance process development, the Mitsunobu reaction had been run at different scales and in various reactor geometries, including round-bottom flasks, laboratory scale cylindrical reactors, and pilot plant reactors. Interestingly, the level of Imp-B was not reproducible from run to run, and it was as high as 9%, as shown in Figure 7. The reaction protocol and the stoichiometry were not varied in these instances.

The formation of Imp-B involves reaction of H_2DIAD with the activated Boc-*L*-Prolinol species (reaction 5). However, the H_2DIAD byproduct is also involved in the crystallization of TPPO−H_2DIAD cocrystals. Therefore, the rate of Imp-B formation depends on the temporal concentration of H_2DIAD in the liquid phase. Irreproducibility in TPPO−H_2DIAD cocrystal formation was postulated to contribute to the variability in Imp-B levels. As H_2DIAD forms in the course of the reaction, at a certain point the formation of TPPO−H_2DIAD cocrystal occurs. The crystallization of the solid byproduct limits the liquid-phase concentration of H_2DIAD. Since primary nucleation can be a stochastic event, the onset of nucleation may be scale- and geometry-dependent, which can result in variable liquid-phase concentrations of H_2DIAD at similar conversions in different experiments. If the onset of nucleation is delayed, it can potentially lead to supersaturation of H_2DIAD and the duration of this supersaturated state can depend on the hydrodynamics in the vessel. In such scenarios, the assumption that the H_2DIAD concentration in the solution phase is equal to the equilibrium concentration may not hold.

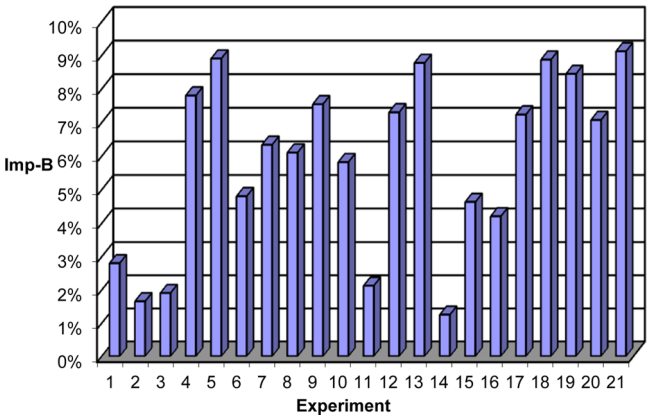

Figure 7. Outcome for Imp-B level from individual Mitsonobu coupling experiments at different scales and in different reactor geometries shows significant variability.

The induction point for nucleation is generally influenced by hydrodynamics in the vessel, which is determined by the mixing, fill-level, and reactor geometry. Since it is difficult to exactly reproduce the hydrodynamics in reactors of different configuration, or even in the same reactor at different fill levels, it is not unreasonable to expect a certain element of variability in nucleation characteristics to be associated with the observed inconsistency in Imp-B formation. We tried to link the variable Imp-B data with conventional mixing parameters such as power/mass, impeller tip speed, impeller shear rate, or 95% mixing time; however, no apparent correlation was obtained with any of these parameters.

In order to track the nucleation and growth of particles during the Mitsunobu reaction under vastly different mixing conditions, Lasentec FBRM was used. The FBRM data were difficult to interpret due to the presence of undissolved pyridinol (reactant) at the outset of the reaction and during the DIAD addition. Therefore, an experiment was designed to separately investigate the nucleation characteristics using a toluene solution saturated with TPPO−H_2DIAD cocrystals at 40 °C in a 250 mL cylindrical reactor equipped with a retreat curve blade impeller. The starting solution, which is clear at 40 °C, was set to cool at a rate of 9 °C/h with an impeller speed of 300 rpm (Expt-A in Figure 8). The first sign of nucleation was observed after 46 min at 34 °C, followed by significant crystallization. The same slurry was heated to dissolve the solids and once again set to cool from 40 °C at a rate of 9 °C/h but with a lower agitation rate of 150 rpm (Expt-B in Figure 8). Interestingly, the induction time for nucleation was extended to 109 min. On the basis of the solubility data for H_2DIAD as a function of temperature, these two nucleation points correspond to a supersaturation ratio of 1.1 and 1.4 for the

DOI: 10.1021/acs.iecr.6b00344
Ind. Eng. Chem. Res. XXXX, XXX, XXX−XXX

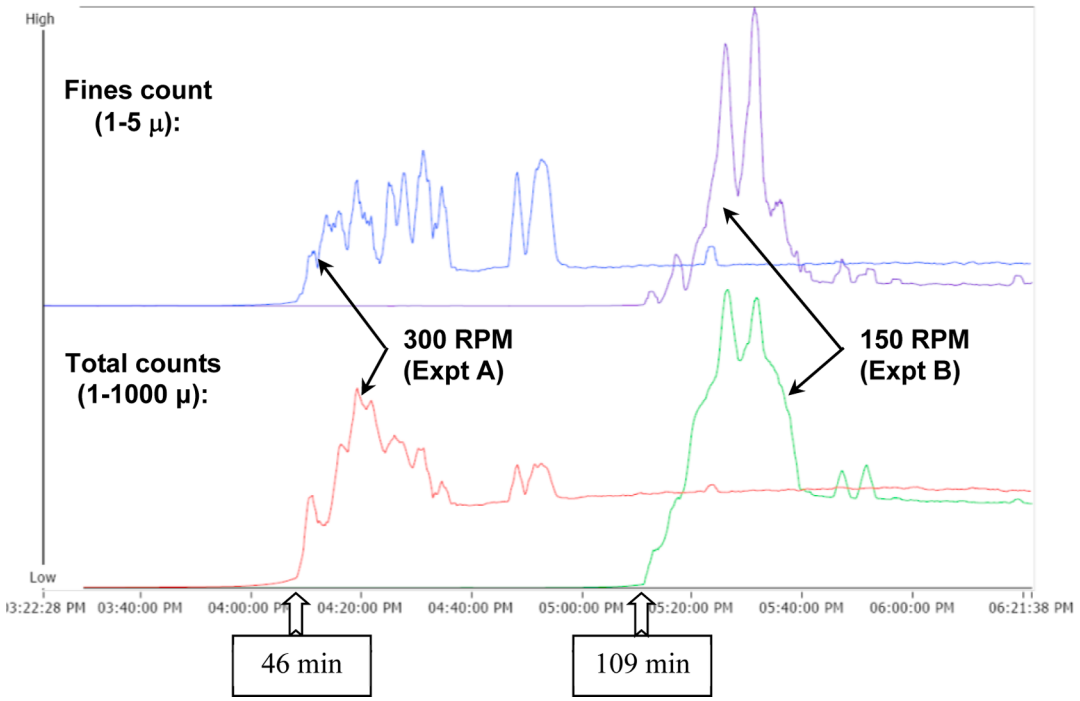

Figure 8. Effect of agitation rate on the onset of nucleation in the TPPO−H_2DIAD system: 300 rpm in Expt A and 150 rpm in Expt B.

experiments at 300 and 150 rpm, respectively. The results from this experiment establish the direct influence of mixing on the induction time for nucleation and, consequently, on the temporal liquid phase concentration of H_2DIAD.

After establishing a link between agitation speed and the onset of TPPO−H_2DIAD cocrystal nucleation, the next step in the investigation was to study the mixing characteristics in the laboratory and pilot plant reactors. As mentioned previously, conventional mixing parameters such as power/mass, impeller tip speed, or impeller shear rate failed to correlate with the variation in Imp-B levels. The above-mentioned conventional mixing parameters are generally useful during process scale up; however, such vessel-averaged mixing parameters do not provide an insight into the microscopic mixing behavior in a vessel.[12] The nucleation of TPPO−H_2DIAD cocrystal is a singular event that is likely to be influenced by the hydrodynamic hot spots in a reactor. The microscopic mixing behavior will vary from reactor to reactor, and even in a given reactor the vessel internals (local geometry) can play a significant role. Nucleation being largely a stochastic event, the local high turbulent energy dissipation rates can significantly increase the probability of nucleation. Hence, it was decided to carry out computational fluid dynamics (CFD) simulations of flow patterns and energy dissipation in the laboratory and pilot plant reactors.

For the CFD simulations, a Reynolds-averaged Navier−Stokes equation based standard k-ε model was employed to describe the turbulence, while the multiple reference frame approach was used to model the impeller rotation. Grid independence studies were carried out to select an appropriate grid size for the computational simulations of each of the configurations to have grid-independent solutions.[13] The CFD simulations, carried out using MixIT software, used the physicochemical properties of toluene (the reaction solvent) at 25 °C and fill levels that are representative of the experiments and production batches. Maps of turbulent energy dissipation rates for a 500-gal pilot plant reactor as shown in Figure 9 indicate a significant spatial difference as a function of agitation speed. The CFD simulation indicates larger regions of high-energy dissipation rates at 100 rpm versus 75 rpm. Also, higher agitation speeds are associated with greater vortexing, as illustrated in Figure 9. The vortex regions close to the impeller shaft tend to have greater gas−liquid phase heterogeneity due to the headspace gas draw that becomes more prominent with an increase in the agitation speed. Such heterogeneous interfaces are generally more conducive for nucleation. Thus, the synergy between higher agitation speeds and greater vortexing should result in favorable conditions for nucleation.

2.4. Hypothesis for Variable Imp-B Formation. A well-controlled mixing study was set up in a 250 mL reactor to investigate the impact of agitation during reaction on the Imp-B level. The results presented in Figure 10 are based on experiments conducted identically in terms of stoichiometry and reaction conditions. Each data point on this plot is a separate experiment, and the Imp-B data presented is the final value when the reaction is complete. The amount of Imp-B formed at lower agitation speed was generally higher, although a sharp decrease in Imp-B is observed at 300 rpm.

Higher agitation rate does not always imply better mixing because the mixing effectiveness may depend on the impeller location in relation to the liquid fill level and, more importantly, the presence of flow diverter elements (vessel internals). In a typical 250 mL or 1 L cylindrical reactor in the laboratory, baffles are not a standard feature, and often a single 1/8th or 1/4th inch diameter thermocouple is the only resistance offered to the flow within the reactor. Therefore, in the absence of baffles, higher agitation may result in marginal improvement in the turbulent energy dissipation. In order to determine the effect of reactor baffling on Imp-B formation, a set of experiments were conducted in standard 1 L cylindrical reactor at different RPMs and in the presence and absence of baffles.[14] The results of the experiments in the 1 L reactor are shown in

DOI: 10.1021/acs.iecr.6b00344
Ind. Eng. Chem. Res. XXXX, XXX, XXX−XXX

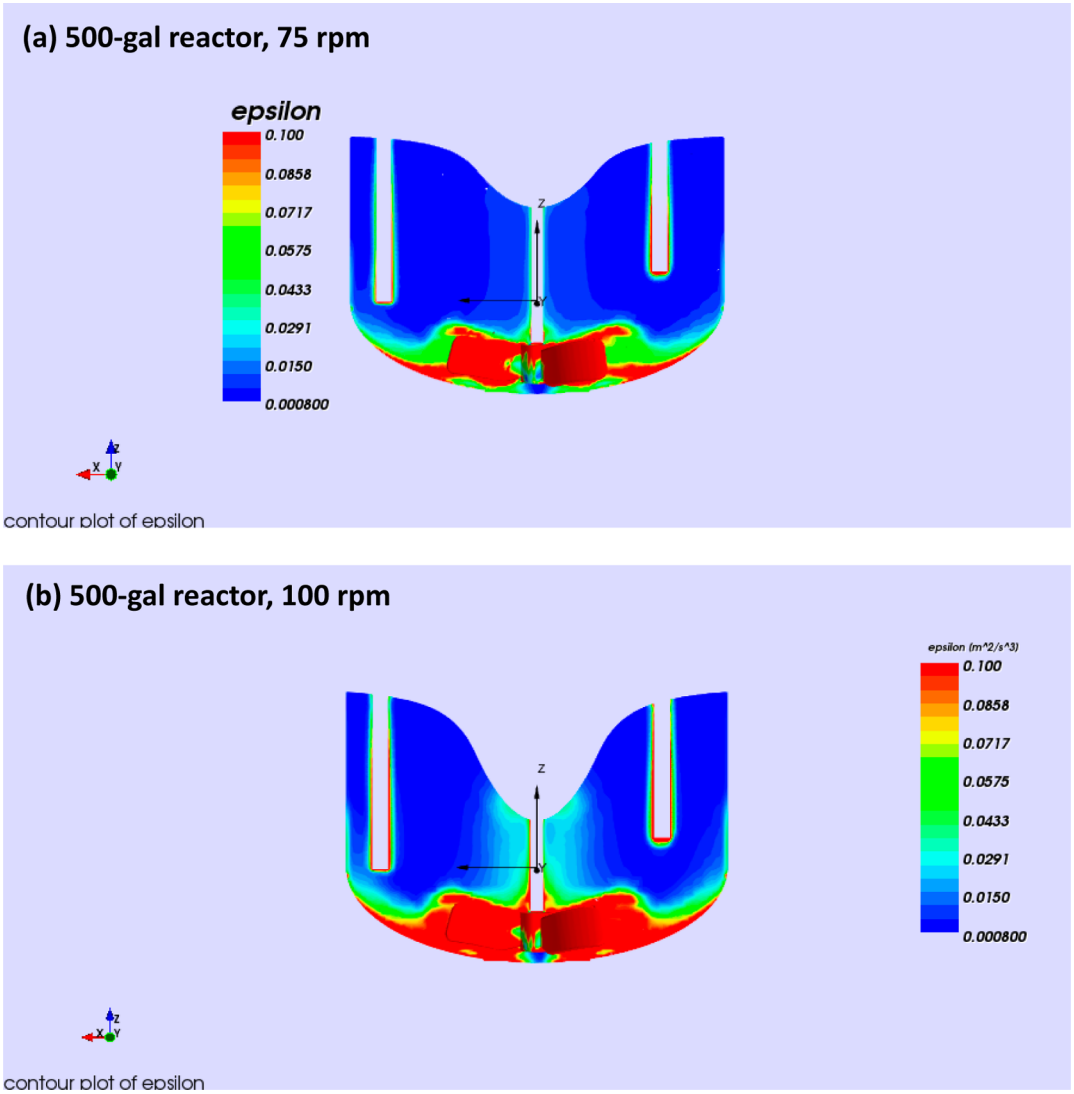

Figure 9. Computational fluid dynamics (CFD) simulation of a 500 gal reactor fitted with a retreat-curve impeller showing the turbulent energy dissipation rate (epsilon) maps at (a) 75 and (b) 100 rpm.

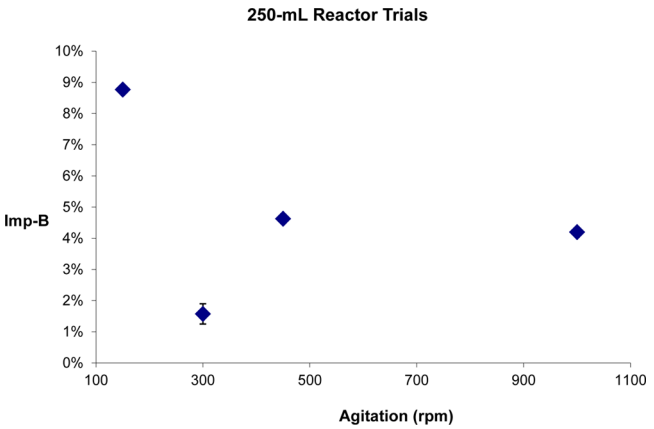

Figure 10. Effect of agitation on Imp-B formation in a 250 mL reactor. The error bar indicates multiple runs conducted at the same agitation.

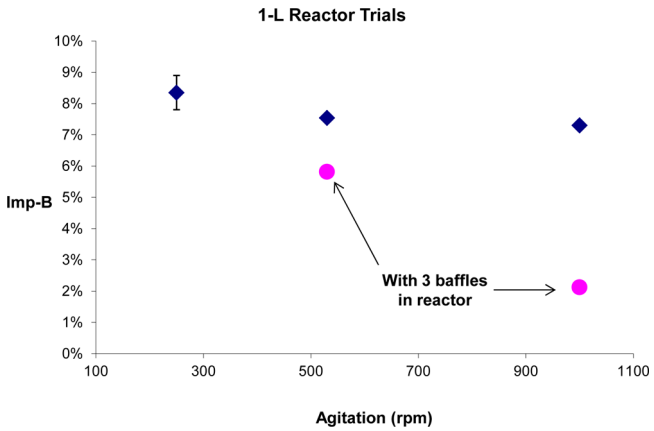

Figure 11. Effect of agitation and baffling on Imp-B formation in a 1 L reactor. The error bar indicates multiple runs conducted at the same agitation.

Figure 11. In the presence of three baffles in the reactor, the Imp-B level at 500 and 1000 rpm were significantly lower than in the absence of baffles. CFD simulations of the 250 mL reactor and the 1 L reactor were conducted to assess the microscopic mixing behavior that can exhibit significant spatial variation in the same reactor with different internals.[15] Figure 12 depicts a greater region of high-turbulent energy dissipation

DOI: 10.1021/acs.iecr.6b00344
Ind. Eng. Chem. Res. XXXX, XXX, XXX−XXX

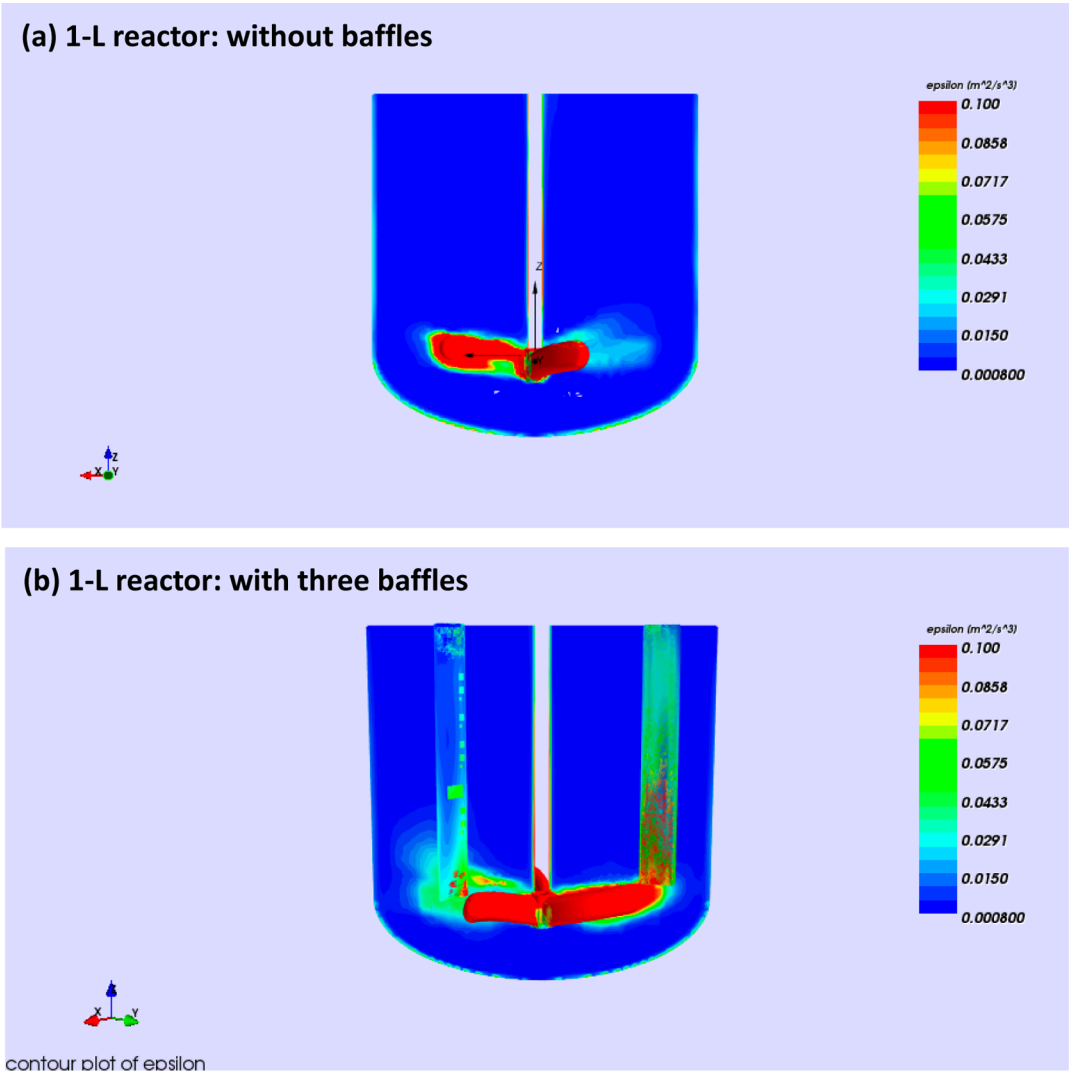

Figure 12. Computational fluid dynamics (CFD) simulation of a 1 L reactor fitted with a retreat-curve impeller showing the turbulent energy dissipation rate (epsilon) maps in the (a) absence and (b) presence of three baffles.

in the presence of the baffles, which is likely a significant contributor for the early nucleation of TPPO−H_2DIAD cocrystal during the reaction. As hypothesized from the reaction understanding and proved experimentally (discussed later in the manuscript), nucleation of the TPPO−H_2DIAD cocrystal limits the liquid-phase concentration of H_2DIAD in the system and thereby decreases the formation of Imp-B.

CFD simulations of the reactors were extremely valuable in understanding the hydrodynamic hot spots as a function of agitation and reactor geometry. In addition to the mixing maps, the CFD simulations were utilized to extract the peak value of the energy dissipation rate for different mixing scenarios to allow a side-by-side comparison, as shown in Table 4. The maximum energy dissipation rate in the 500 gal reactor is increased by about 50% when agitation speed is increased from 75 to 100 rpm, and an even higher increase is noted in the 250 mL reactor going from 150 to 300 rpm. The presence of baffles in the 1 L reactor significantly increases the maximum energy dissipation rate at agitation speeds of 500 and 1000 rpm. Therefore, when the energy dissipation rates are drastically improved through baffling and high agitation, the onset of TPPO−H_2DIAD cocrystal nucleation is relatively faster, resulting in lower levels of Imp-B.

Table 4. Comparison of the Maximum Energy Dissipation Rate Derived from CFD Simulations for Various Reactors

reactor	agitation (rpm)	number of baffles	maximum energy dissipation rate (m^2/s^3)
250 mL	150	none	2.0
	300	none	4.8
1 L	500	none	13.4
		3	23.6
	1000	none	101.9
		3	198.0
500 gal	75	one dip-tube and one beavertail baffle	18.5
	100	one dip-tube and one beavertail baffle	29.9

In order to confirm the hypothesis that early nucleation of the TPPO−H_2DIAD cocrystal minimizes the formation of Imp-B, TPPO was intentionally added to the coupling reaction to induce nucleation of the cocrystal. The solubility of H_2DIAD was measured in a separate experiment by adding ca. 0.85 mol equiv of TPPO to an already saturated TPPO−H_2DIAD solution. As shown in Figure 13, the solubility data confirm that

DOI: 10.1021/acs.iecr.6b00344
Ind. Eng. Chem. Res. XXXX, XXX, XXX−XXX

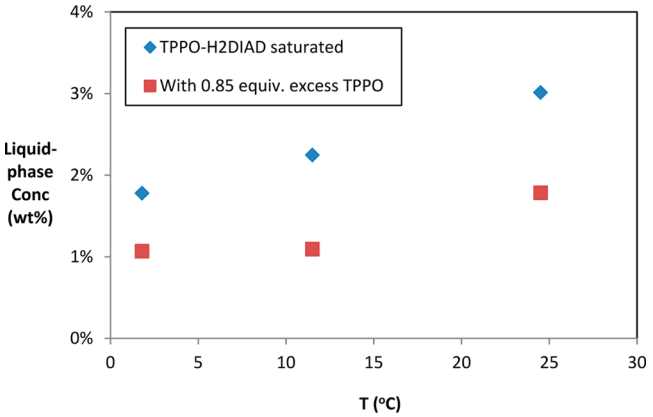

Figure 13. Influence of excess TPPO on H_2DIAD equilibrium concentration in the reaction medium.

TPPO spiking leads to cocrystal formation, which causes a substantial decrease in the liquid-phase concentration of H_2DIAD consistently across the temperature range of interest. On the basis of this information, an experiment was carried out in a 250 mL reactor where 0.85 equiv of TPPO was added to the typical reaction charges (Boc-*L*-prolinol, pyridinol, TPP, and DIAD). Interestingly, the TPPO-spiked experiment resulted in 3.1% of Imp-B, which is about 30% lower than the 4.6% observed in a control experiment using the same set up and same protocol.

The above studies indicate that high intensity mixing as well as addition of TPPO to the reaction induces nucleation of the TPPO−H_2DIAD cocrystal. Consequently, this limits the solution concentration of H_2DIAD and minimizes the formation of Imp-B.

3. CONCLUSIONS

The initial investigation on the Mitsunobu coupling was focused on understanding the formation of different process impurities, especially Imp-B, through the development of the kinetics model. Imp-A and the isomer impurity were determined to be easily managed by restricting the stoichiometry of the reagents: TPP:DIAD > 1 and pyridinol:TPP < 1. With regard to Imp-B formation, one of the reaction byproducts, H_2DIAD, is a precursor, which crystallizes out during the reaction, thus limiting the available concentration for impurity formation. Interestingly, H_2DIAD forms a cocrystal with another reaction byproduct, TPPO, as evidenced from the distinct powder XRD pattern of the combined entity compared to the individual components.

A reaction mechanism was proposed and a fit-for-purpose kinetics model was established that accounted for the variable H_2DIAD concentration in the system. When the historical data on the reaction was assessed, it was observed that the level of Imp-B was variable under the nominal operating conditions (stoichiometry, temperature, and protocol) when changes in scale and/or reactor geometry were made. Through a set of targeted experiments, it was shown that mixing intensity during the reaction had a significant bearing on the resulting Imp-B level. While in a typical case, mixing is characterized by an operating parameter such as agitation speed, or a scale-independent mixing parameter such as power/mass; in this study, we could not find a direct correlation of Imp-B level to any one mixing parameter. CFD simulations on 1 L reactor with and without baffles provided significant insights into the local mixing pattern, which significantly influences the nucleation characteristics of the TPPO−H_2DIAD cocrystal. It was also separately established that mixing intensity had a direct impact on the induction time of the cocrystal nucleation. The role of cocrystal formation in reducing the equilibrium concentration of H_2DIAD was established by spiking TPPO to the reaction, which resulted in lower Imp-B formation. Since variability in Imp-B formation was linked to the nucleation behavior of the TPPO−H_2DIAD cocrystal, it is paramount to employ well-characterized vessels with good mixing capability to control the nucleation of the TPPO−H_2DIAD cocrystal and thereby minimize the level of Imp-B.

AUTHOR INFORMATION

Corresponding Author

*E-mail: samrat.mukherjee@abbvie.com.

Notes

The authors declare no competing financial interest.

ACKNOWLEDGMENTS

This study was sponsored by AbbVie Inc. AbbVie contributed to the design, research, and interpretation of data, writing, reviewing, and approving the publication. All authors are AbbVie employees.

REFERENCES

(1) Mitsunobu, O. The use of diethyl azodicarboxylate and triphenylphosphine in synthesis and transformation of natural products. *Synthesis* **1981**, *1981*, 1.

(2) Refs 3−14 from the review paper by Kumara: Swamy, K. C.; Bhuvan Kumar, N. N.; Balaraman, E.; Pavan Kumar, K. V. P. Mitsunobu and Related Reactions: Advances and Applications. *Chem. Rev.* **2009**, *109*, 2551−2651.

(3) Camp, D.; Jenkins, I. D. The mechanism of the Mitsunobu esterification reaction. Part I. The involvement of phosphoranes and oxyphosphonium salts. *J. Org. Chem.* **1989**, *54*, 3045.

(4) Camp, D.; Jenkins, I. D. The mechanism of the Mitsunobu esterification reaction. Part II. The involvement of (acyloxy)-alkoxyphosphoranes. *J. Org. Chem.* **1989**, *54*, 3049.

(5) Hughes, D. L.; Reamer, R. A.; Bergan, J. J.; Grabowski, E. J. J. A Mechanistic Study of the Mitsunobu Esterification Reaction. *J. Am. Chem. Soc.* **1988**, *110*, 6487−6491.

(6) Shi, J. Y.; Hughes, D. L.; McNamara, J. M. Stereospecific synthesis of chiral tertiary alkyl-aryl ethers via Mitsunobu reaction with complete inversion of configuration. *Tetrahedron Lett.* **2003**, *44*, 3609.

(7) Guanti, G.; Banfi, L.; Basso, A.; Bevilacqua, E.; Bondanza, L.; Riva, R. Efficient chemoenzymatic enantioselective synthesis of diacylglycerols (DAG). *Tetrahedron: Asymmetry* **2004**, *15*, 2889.

(8) Varasi, M.; Walker, K. A. M.; Maddox, M. L. A Revised Mechanism for the Mitsunobu Reaction. *J. Org. Chem.* **1987**, *52*, 4235.

(9) Wada, M.; Mitsunobu, O. Intermolecular dehydration between alcohols and active hydrogen compounds by means of diethyl azodicarboxylate and triphenylphosphine. *Tetrahedron Lett.* **1972**, *13*, 1279.

(10) Etter, M. C.; Baures, P. W. Triphenylphosphine Oxide as a Crystallization Aid. *J. Am. Chem. Soc.* **1988**, *110*, 639−640.

(11) Ideally, at the nucleation point, a step-change in the liquid phase TPPO or H_2DIAD concentration to its respective equilibrium concentration for the cocrystal is expected. However, the TPPO or H_2DIAD concentration plots in Figure 6b indicate a decrease over 60 min (as opposed to a step-change) due to an artifact related to the frequency of sampling.

(12) Nere, N. K.; Patwardhan, A. W.; Joshi, J. B. Liquid-Phase Mixing in Stirred Vessels: Turbulent Flow Regime. *Ind. Eng. Chem. Res.* **2003**, *42*, 2661.

DOI: 10.1021/acs.iecr.6b00344
Ind. Eng. Chem. Res. XXXX, XXX, XXX−XXX

(13) Joshi, J. B.; Nere, N. K.; Rane, C. V.; Murthy, B. N.; Mathpati, C. S.; Patwardhan, A. W.; Ranade, V. V. CFD simulation of stirred tanks: comparison of turbulence models. Part I: radial flow impellers. *Can. J. Chem. Eng.* **2011**, *89*, 23.

(14) Baffles were inserted from top of the 1 L reactor. The 250 mL reactor was not amenable to baffles due to the small cross section of the reactor.

(15) Kumaresan, T.; Nere, N. K.; Joshi, J. B. Effect of Internals on the Flow Pattern and Mixing in Stirred Tanks. *Ind. Eng. Chem. Res.* **2005**, *44*, 9951.

DOI: 10.1021/acs.iecr.6b00344
Ind. Eng. Chem. Res. XXXX, XXX, XXX−XXX